Article

In-situ Generation of Azonia-containing Polyelectrolytes for Luminescent Photopatterning and Superbug Killing

Xiaolin Liu, Mengge Li, Ting Han, Bing Cao, Zijie Qiu, Yuanyuan Li, Qiyao Li, Yubing Hu, Zhiyang Liu, Jacky W. Y. Lam, Xianglong Hu, and Ben Zhong Tang

J. Am. Chem. Soc., **Just Accepted Manuscript** • DOI: 10.1021/jacs.9b04757 • Publication Date (Web): 20 Jun 2019

In-situ Generation of Azonia-containing Polyelectrolytes for Luminescent Photopatterning and Superbug Killing

Xiaolin Liu,[†,§,#] Mengge Li,[‡,#] Ting Han,[†,§] Bing Cao,[‡] Zijie Qiu,[†,§] Yuanyuan Li,[†,§] Qiyao Li,[†,§] Yubing Hu,[†,§] Zhiyang Liu,[†,§] Jacky W. Y. Lam,[†,§,*] Xianglong Hu,[‡,*] Ben Zhong Tang[†,§,‖,*]

[†] Department of Chemistry, Hong Kong Branch of Chinese National Engineering Research Center for Tissue Restoration and Reconstruction, Institute for Advanced Study, Department of Chemical and Biological Engineering, Institute of Molecular Functional Materials, The Hong Kong University of Science and Technology, Clear Water Bay, Kowloon, Hong Kong, China

[‡] Ministry of Education Key Laboratory of Laser Life Science & Institute of Laser Life Science, College of Biophotonics, South China Normal University, Guangzhou 510631, China

[§] HKUST-Shenzhen Research Institute, No. 9 Yuexing 1st RD, South Area, Hi-tech Park, Nanshan, Shenzhen 518057, China

[‖] Center for Aggregation-Induced Emission, SCUT-HKUST Joint Research Institute, State Key Laboratory of Luminescent Materials and Devices, South China University of Technology, Guangzhou 510640, China

ABSTRACT: Polyelectrolytes play important role in both natural biological systems and human society, and their synthesis, functional exploration, and profound application are thus essential for biomimicry and creating new materials. In this study, we developed an efficient synthetic methodology for in-situ generation of azonia-containing polyelectrolytes in a one-pot manner by using readily accessible nonionic reactant in the presence of commercially available cheap ionic species. The resulting polyelectrolytes are emissive in the solid state, and can readily form luminescent photopatterns with different colors. The azonia-containing polyelectrolytes possess extraordinary potency of reactive oxygen species (ROS) generation, enabling them to impressively kill methicillin-resistant *Staphylococcus aureus* (MRSA), a drug resistant superbug, both *in vitro* and *in vivo*.

INTRODUCTION

Many important biological macromolecules are polyelectrolytes, such as DNA, proteins, polypeptides and polysaccharides.[1-3] Polyelectrolytes are ionizable polymers possessing the combined behaviors of polymers and electrolytes, which can drastically change the fluid properties of aqueous solutions, interact with oppositely charged macromolecules, small ions, and even neutral particles. Polyelectrolytes have demonstrated great potency in many aspects, for example, thickening agents in food industry, waste water treatment in environment science, diagnostic and therapeutic agents in medicine.[4-5] For biomimicry and creating new materials, it is attractive to synthesize and study polyelectrolytes. However, the progress is unsatisfactory because of their synthetic difficulty.[6] The main methodology for the synthesis of polyelectrolytes is post-modification of nonionic polymers.[7-9] One archetype example is sodium polystyrene sulfonate (NaPSS), which is synthesized by adding sulfonate groups after polymerization.[10-11] Another typical example is polyacrylic acid (PAA), which is generally obtained by the hydrolysis of polyacrylate.[12-13] Theoretically, the post-modifications are hard to be 100% completed, allowing patches along the polymer chain, which are impossible to be removed and purified. Some coupling reactions (Heck[14] and Sonogashira[15]) are also employed for the synthesis of polyelectrolytes but they frequently require expensive and limited types of ionic monomers.

Most commercially available polyelectrolytes (such as NaPSS and PAA) are commodity polymers, which are cheap and useful in daily life but show no advanced functional properties.[16-17] Specialty polymers (such as conducting polymers, liquid crystalline polymers, and biomedical polymers) are attracting much interest because of their novel functionalities.[18-23] There are some progresses in developing specialty polyelectrolytes, with water-soluble conjugated polymers being a typical example. A plenty of water-soluble conjugated polymers have been designed and synthesized for bio-imaging, diagnosis and therapy,[24-28] using their fluorescence and photodynamic properties. However, traditional specialty polymers often suffer from aggregation-caused quenching effect in the condensed state, which significantly decreases their emission efficiency or intersystem crossing (ISC) efficiency because

of the high probability of the excited state to undergo nonradiative relaxation.[29] As it is hard to completely avoid aggregation in diverse practical applications, new specialty polyelectrolytes are in great demand to address these problems.[30]

In our previous work, some azonia aromatic compounds have been found to show aggregation-induced emission (AIE) characteristics with strong reactive oxygen species (ROS) generation ability.[31-34] The azonia rings are highly electron-deficient, and they are thus easy to form donor-acceptor (D-A) structures with tunable emission color by combining with different electron donors.[35] Many reported antibiotics are also azonia-containing molecules but the processability of these small molecules is quite limited.[36] Thus, we intend to combine the excellent performance of azonia aromatic compounds with processable polymers to create new functional materials with expectable optical properties and processability. The resulting azonia-containing polyelectrolytes are expected to show good processing ability that can be easily fabricated into luminescent films for applications in surface modification, patterning and large area display system. With high charge density in the polymer chain, the azonia-containing polyelectrolytes may show affinity to negative charge species (such as bacteria membrane and DNA), which enable them to wrap the surface of bacteria and physically kill them.[4, 37-38] By introducing D-A structure into the polyelectrolytes, the nonradiative decay channel is blocked due to the rigid structure,[29] which is beneficial for bioimaging and ROS generation. As a result, the azonia-containing polyelectrolytes are potential powerful weapons to kill superbugs by photodynamic therapy besides physically killing.[39-40]

Owing to the attractive properties of azonia aromatic compounds, many novel approaches have been developed for the synthesis of azonia small molecules,[41] including ring-closing metathesis reactions,[42-43] annulation reactions based on C-H activation,[44-46] and so on. But it is challenging to develop these small molecule reactions for polymer synthesis due to the limited organic reactions with mild reaction condition, broad monomer scope and high efficiency. In 2017, Jun et al. reported an efficient method for the synthesis of benzoquinolizinium salts in a one-pot manner from simple starting materials (Scheme 1A).[47] Inspired by this work, we try to develop such efficient small molecule reaction into useful tool for the synthesis of azonia-containing polyelectrolyte.

In this study, we developed a synthetic methodology by readily accessible nonionic reactant in the presence of commercially available cheap ionic species to in-situ generate azonia-containing polyelectrolytes in a one-pot manner. The main-chain polyelectrolytes were generated in excellent yields (up to 99%) with high molecular weights (up to 28 700 Da). The azonia-containing polyelectrolytes were luminescent in the solid state with good processing ability, which enabled them to be excellent candidate materials for fluorescent photopattern generation. With extraordinary strong ROS generation ability, these polyelectrolytes could impressively solve the bacterial resistance issue. Systematic antibacterial explorations were conducted, including bacteria staining and killing methicillin-resistant *Staphylococcus aureus* (MRSA), a drug resistant superbug *in vitro* and *in vivo*.

Scheme 1. Synthesis of azonia-containing polyelectrolytes

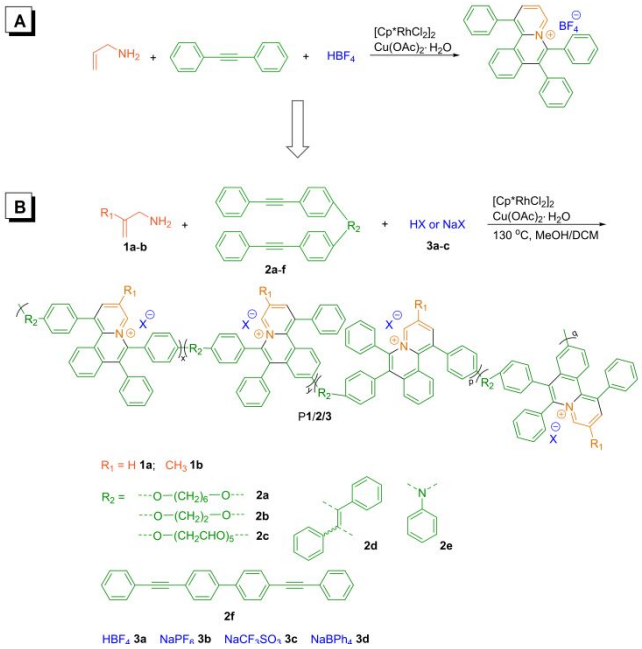

RESULTS AND DISCUSSION

Polymerization. Monomers used in this work are easily available. Allylamines **1a**–**b**, tetrafluoroboric acid (HBF_4, **3a**), sodium hexafluorophosphate ($NaPF_6$, **3b**), sodium trifluoromethanesulfonate ($NaCF_3SO_3$, **3c**), sodium tetraphenylborate ($NaBPh_4$, **3d**), sodium tetrafluoroborate (HBF_4), and hexafluorophosphoric acid (HPF_6) were commercially available and used without further purification. The internal diynes **2a**–**h** used in this work were readily synthesized without column chromatography purification. All the polymerizations were catalyzed by $[Cp^*RhCl_2]_2$ and $Cu(OAc)_2{\cdot}H_2O$ and conducted under air atmosphere in a one-pot manner.

To obtain soluble polyelectrolytes with high molecular weights in high yields, we systematically investigated the polymerization conditions using **1a**, **2a** and **3a** as monomers. The solvent, monomer ratio, catalyst loading, concentration, and reaction time were carefully investigated (Table 1). The effect of solvent on the polymerization was first investigated (entries 1–5, Table 1). Polar solvents such as MeOH, DCM, MeOH/DMSO, and MeOH/DCM mixed solvents were investigated and the best polymerization result was obtained in MeOH/DCM (v/v, 1/1), affording polymer with M_w of 19 200 Da in 72% yield (entry 5, Table 1). It was found that monomer ratio (entries 5–6, Table 1) exerted little effect on the polymerization, while the catalyst loading (entries 5, and 7–9, Table 1) played a crucial role in the polymerization. Decreasing the amount of $[Cp^*RhCl_2]_2$ from 10 mol% to 5 mol% even increased the M_w and yield (entry 7, Table 1), but further reducing the loading of $[Cp^*RhCl_2]_2$ or $Cu(OAc)_2{\cdot}H_2O$ led to a sharp decrease in both the values of M_w and yield. With the optimized catalyst loading, we further investigated the

Table 1. Optimization of the polyannulation reaction[a]

entry	solvent	[**1a**] (M)	[**2a**] (M)	[Rh] (%)	[Cu] (equiv)	yield (%)	M_n[b]	M_w[b]	M_w/M_n[b]
1	MeOH	0.20	0.20	10	5	trace			
2[c]	MeOH/DMSO	0.20	0.20	10	5	trace			
3[c]	MeOH/DMSO	0.20	0.20	10	5	trace			
4	DCM	0.20	0.20	10	5	54	7 600	13 700	1.8
5	MeOH/DCM	0.20	0.20	10	5	72	14 800	19 200	1.3
6	MeOH/DCM	0.20	0.25	10	5	87	12 700	16 500	1.3
7	MeOH/DCM	0.20	0.20	5	5	93	20 400	28 700	1.4
8	MeOH/DCM	0.20	0.20	2.5	5	4	4 500	4 900	1.1
9	MeOH/DCM	0.20	0.20	5	2.5	trace			
10	MeOH/DCM	0.25	0.25	5	5	85	15 800	20 500	1.3
11	MeOH/DCM	0.15	0.15	5	5	72	6 400	9 600	1.5
12[d]	MeOH/DCM	0.20	0.20	5	5	70	12 400	16 100	1.3
13[d]	MeOH/DCM	0.20	0.20	5	5	21	6 700	8 700	1.3
14[e]	MeOH/DCM	0.20	0.20	5	5	47	3 500	7 900	2.3

[a]Unless otherwise noted, the polymerizations were carried out at 130 °C in air for 24 h, [**3a**] = 0.3M, in MeOH, DCM or their mixture (1:1). [b]Estimated by GPC in DMF on the basis of a linear polystyrene calibration. [c]MeOH/DMSO = 8:2 (entry 2), and 6:4 (entry 3). [d]Reaction time was 18 h (entry 12) and 12 h (entry 13). [e]$NaBF_4$ was used instead of HBF_4.

effect of monomer concentration and reaction time on the polymerization. When the monomer concentration of **1a** was decreased from 0.2 M to 0.15 M, both the M_w and yield decreased sharply (entry 11, Table 1). When the monomer concentration of **1a** was improved from 0.2 M to 0.25 M, the M_w and yield decreased slightly, with partial gelation occurred (entry 10, Table 1). 24 h was adopted as the optimal reaction time, as further decrease of the reaction time led to unsatisfactory values of M_w and yield (entries 12–13, Table 1).

Table 2. Polyannulation results of different monomers[a]

entry	monomer	yield (%)	M_n[b]	M_w[b]	M_w/M_n[b]
1	**1a/2a/3a**	93	20 400	28 700	1.4
2	**1a/2b/3a**	60	11 900	14 900	1.3
3[c]	**1a/2c/3a**	99	17 900	24 000	1.3
4	**1a/2d/3a**	71	14 000	20 000	1.4
5	**1a/2e/3a**	74	18 900	22 700	1.2
6[d]	**1a/2f/3a**	78	5 700	8 100	1.4
7[d]	**1b/2a/3a**	52	17 700	26 000	1.5
8	**1b/2e/3a**	53	18 800	23 700	1.3
9	**1a/2a/3b**	64	13 100	21 500	1.6
10[d]	**1a/2a/3c**	75	16 800	25 100	1.5
11	**1a/2a/3d**	25	5 600	7 600	1.3

[a]Unless otherwise noted, the polymerizations were carried out at 130 °C in air for 24 h, [**1**] = [**2**] = 0.2 M, [**3**] = 0.3 M, [Rh] = 5 mol%, [Cu] = 5 equiv. Solvent: DCM/MeOH=1:1. [b]Estimated by GPC in DMF on the basis of a linear polystyrene calibration. [c]Reaction time was 36 h. [d]Partially insoluble.

With the optimized polymerization conditions in hand, different monomer combinations were applied to test the robustness and wide applicability of this polymerization route (Table 2). Monomers **2a**–**c** were internal diynes with flexible alkyl chain or oxyalkyl chain as spacer, while **2d**–**f** were rigid conjugated diynes with different electron density. Monomers **3a**–**d** were abundant and cheap acid or salt. Diyne **2a**–**f** all reacted efficiently with **1a** and **3a**, affording polyelectrolytes with high yield and molecular weight (entries 1–6, Table 2). The diarylacetylene structure was crucial for this polymerization, as only a trace amount of product was obtained when tert-butyl-substituted diyne **2g** (Scheme S1) was used as diyne monomer to react with **1a** and **3a**. The fluorene-substituted diyne **2h** (Scheme S1) also failed to be polymerized effectively, probably due to the large steric hindrance of fluorene moiety. Regarding the monomer scope of allylamines, both unsubstituted allylamine **1a** or methyl-substituted allylamine **1b** could react efficiently with diyne **2a** or **2e** in the presence of **3a** (entries 1–2, 7–8, Table 2). But **1b** was less reactive compared to **1a**, which was probably due to the steric hindrance of the methyl group. Finally, we further explored the influence of ion source on the polymerization process. Based on the mechanism of small molecules,[47] we proposed a mechanism of the polymerization route (Scheme S3). In the proposed mechanism, the ion source could react with the seven-membered rhodacycle complex **D** to form benzoquinolizium salt, which was crucial to the polymerization. We had demonstrated that HBF_4 **3a**, $NaPH_6$ **3b** and $NaCF_3SO_3$ **3c** could react efficiently with **1a** and **2a** to generate polyelectrolytes with moderate M_w and yield (entries 1, 9–10, Table 2), while the $NaBPh_4$ **3d** was much less reactive with **1a** and **2a** (entries 11, Table 2), presumably resulting from the steric hindrance. HPF_6 failed to polymerize with **1a** and **2a**, probably due to the too

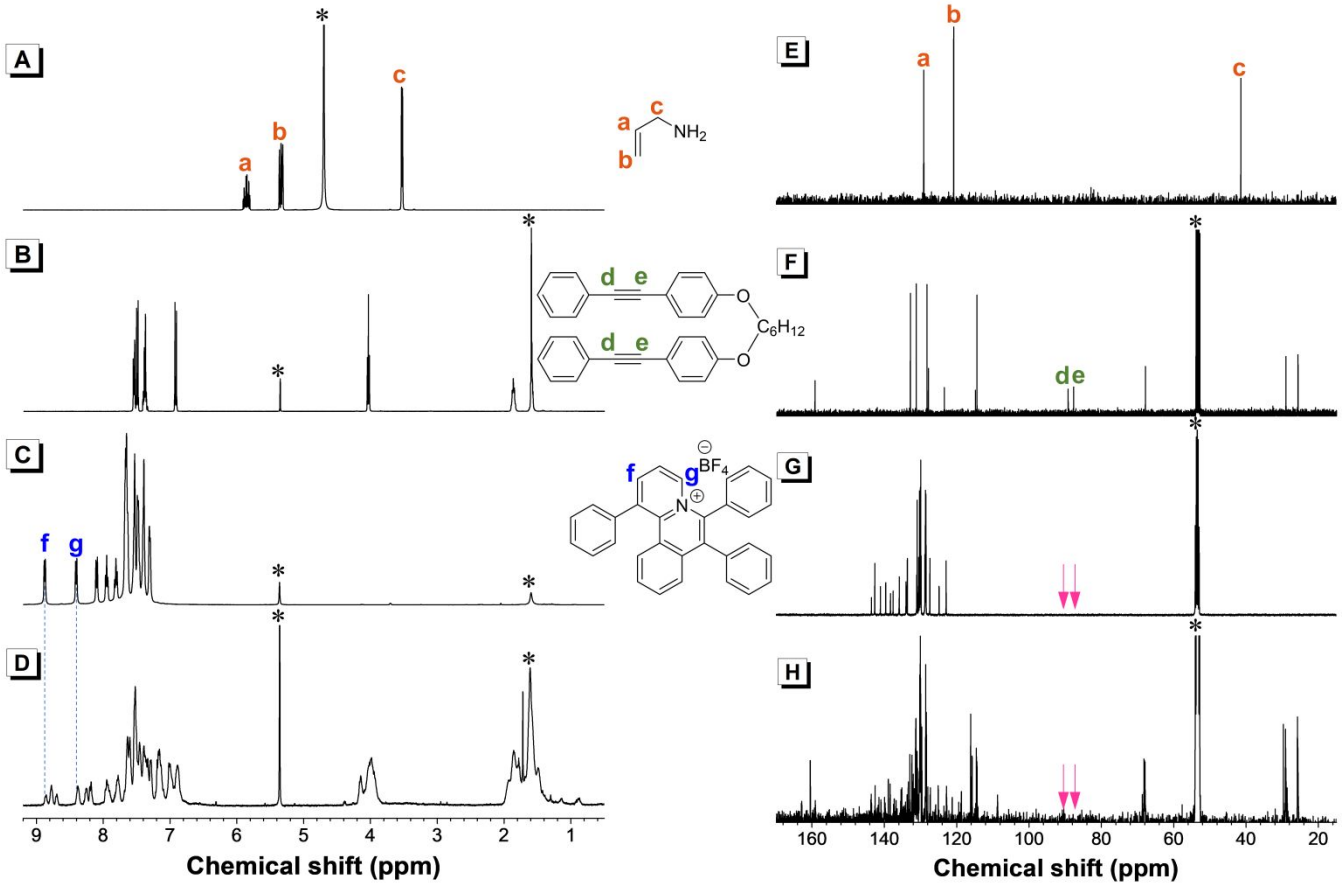

Figure 1. ^{1}H NMR spectra of (A) **1a** in D_2O and (B) **2a**, (C) model compound **2** and (D) **P1a/2a/3a** in CD_2Cl_2. ^{13}C NMR spectra of (E) **1a** in D_2O and (F) **2a**, (G) model compound **2** and (H) **P1a/2a/3a** in CD_2Cl_2.

strong acidity or decomposition upon heating of HPF_6. These results indicated that we successfully developed an efficient and powerful polymerization tool for the construction of azonia-containing polyelectrolytes. The only byproduct produced from this polymerization was hydrogen ion, indicating its high atom economy.

Most of the obtained polyelectrolytes showed good solubility in commonly used organic solvents, such as DCM, chloroform, DMSO, and *N*,*N*-dimethylformamide (DMF), whereas P**1b/2a/3a** and P**1a/2a/3c** were partially insoluble in these solvents. The thermal properties of the polyelectrolytes were evaluated by thermogravimetric analysis (TGA), and the results indicated that the 5% weight loss temperatures (T_d) were in the range of 218–323 °C (Figure S4), suggesting that they were thermally stable. Additionally, P**1a/2d/3a** and P**1a/2e/3a** displayed 70% of their weight even upon heating to 800 °C.

Structural Characterization. The structures of the resulting polymers were characterized by FT-IR and NMR spectra. To gain insight into the structures of these azonia-containing polyelectrolytes, model compound **2** was prepared by cascade double *N*-annulation reaction of allylamine **1a**, diphenylacetylene **1**, and HBF_4 under the same synthetic conditions for the polyelectrolytes (Scheme S2). Typical FT-IR analysis and ^{1}H NMR and ^{13}C NMR spectra of polymer P**1a/2a/3a**, model compound **2**, and their corresponding monomers **1a** and **2a** were performed accordingly for further illustration. In the FT-IR spectra (Figure S1), the N-H stretching vibration of **1a** and the C≡C stretching vibrations of **2a** occurred at 3012 and 2220 cm^{-1}, respectively. These peaks could not be observed in the spectra of P**1a/2a/3a** and **2**. Meanwhile, a new peak associated with B-F stretching vibrations appeared at 1083 cm^{-1}, indicating the successful occurrence of the reaction. Similar results were obtained in the FT-IR spectra of other polymers (Figure S2-3).

In addition, NMR spectra could provide more detailed information about the polymer structures. In the ^{1}H NMR spectra, the protons at position "a", "b" and "c" of **1a** resonate at δ 5.95 ppm, 5.43 ppm and 3.63 ppm, respectively, disappeared in the ^{1}H NMR spectra of P**1a/2a/3a** and **2**. Most importantly, new peaks emerged at δ 8.84 ppm and 8.37 ppm in the spectra of P**1a/2a/3a** and **2**, corresponding to the aromatic protons from the newly formed benzoquinolizinium rings (Figure 1A–D). The ^{13}C NMR spectra further verified the polymer structure (Figure 1E–H). The characteristic peaks of C≡C in **2a** was not observed in the polymer spectrum. Instead, the aromatic carbon on benzoquinolizinium rings resonated at δ 143–120 ppm in the spectra of P**1a/2a/3a** and **2**. For all the 10 polyelectrolytes, the characteristic peaks at δ 8.90–8.10 ppm all emerged in their ^{1}H NMR spectra, and their characteristic C≡C peaks at δ 90.0–88.0 ppm all disappeared in their ^{13}C NMR spectra, confirming successful fabrication of their azonia-containing polyelectrolytes accordingly (Figure S22–48).

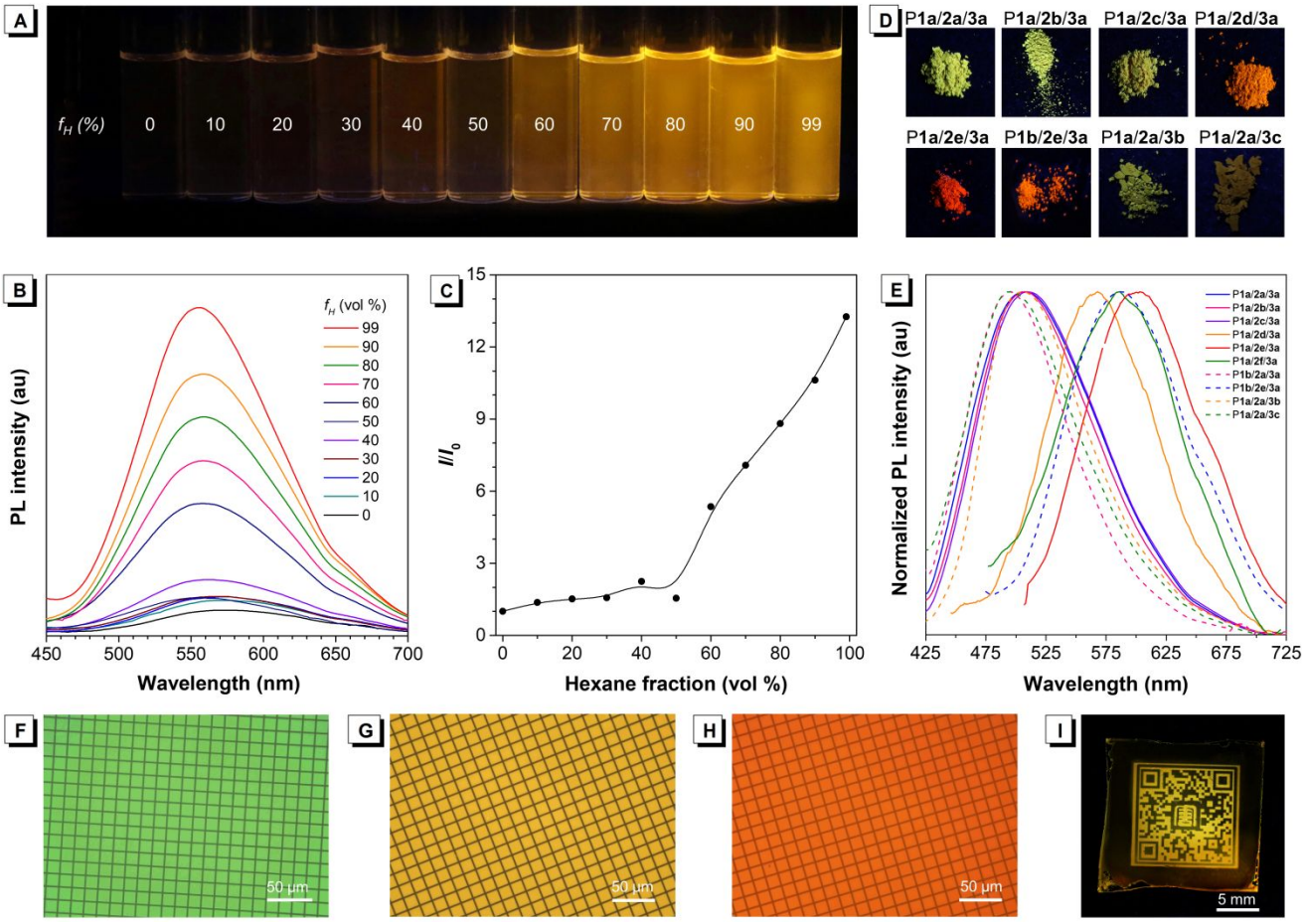

Figure 2. (A) Photographs of P**1a/2d/3a** in DCM/hexane mixtures with different hexane fractions (f_H) taken under 365 nm UV irradiation from a handheld UV lamp. (B) Emission spectra of P**1a/2d/3a** in DCM/hexane mixtures with different hexane fractions. Excitation wavelength: 380 nm. (C) Plot of relative emission intensity (I/I_0) versus the composition of the DCM/hexane mixture of P**1a/2d/3a**. Solution concentration: 10 μM. (D) Luminescent photographs of polymer P**1/2/3** in the solid state. (E) Emission spectra of thin films of P**1/2/3**. Excitation wavelength: 450 nm for P**1a/2e/3a**, and 380 nm for the other polymers. (F-I) Two-dimensional fluorescent photopatterns generated by photolithography of films of (F) P**1a/2a/3a**, (G) P**1a/2d/3a**, (H) P**1a/2e/3a**, and (I) P**1a/2d/3a** taken under UV irradiation. Excitation wavelength: 330–385 nm.

Photoluminescence (PL) Properties and Photopattern. The absorption and emission spectra of dilute DCM solutions (10 μM) of the resulting azonia-containing polyelectrolytes were shown in Figure S6-7. Due to the strong electron-withdrawing azonia aromatic moiety, the maximum emission wavelength of these polymers was facilely tunable from 490 to 610 nm, arised from the polymerization from diyne monomers with different electron density.

By incorporating TPE and TPA moiety into the polyelectrolyte skeletons respectively, the resulting polymer P**1a/2d/3a** and P**1a/2e/3a** showed typical AIE features. Taking P**1a/2d/3a** as an example, its DCM solution emitted weakly at 574 nm. With the addition of hexane, a non-polar poor solvent for the polymer, the emission intensity gradually increased, the photographs of these dispersions taken in DCM/hexane mixtures with different hexane fractions visually showed the trends in fluorescence (Figure 2A), and the maximum emission wavelengths slightly blue-shifted to 558 nm (Figure 2B). The PL intensity of P**1a/2d/3a** aggregates in DCM/hexane mixture with 99% hexane fraction (I_{99}) was ~13-fold higher than that in pure DCM solution (I_0) (Figure 2C). Similar phenomenon was observed for P**1a/2e/3a** (Figure S9).

After that, the solid fluorescence of these azonia-containing polyelectrolytes were examined (Figure 2D), all these polymers were emissive in solid state. P**1a**–**b**/**2a**–**c**/**3a**–**b** displayed yellow-green emission, P**1a/2d/3a** and P**1b/2e/3a** emitted orange fluorescence, and P**1a/2e/3a** exhibited red emission. PL spectra of these polymers in solid state were further performed (Figure 2E). Because of the excellent solubility and film-forming ability of P**1/2/3**, their uniform films could be easily fabricated without defect on silica wafers by a simple spin-coating technique.

Macroscopically processable polymers with high refractive indices (RI) are promising candidate materials for various photonic applications, including optical chips, prisms, optical waveguides, memories and holographic image recording systems.[48] Since multi-fused heterocyclic rings were incorporated in the polymer main-chain, the azonia-containing polyelectrolytes are expected to show high refractive index. The thin films of P**1/2/3** were

prepared by spin-coating and their refractive indexes were measured accordingly. As summarized in Figure S8 and Table S1, their thin films indeed showed high *n* values of 1.817–1.600 in the spectral regin of 400–900 nm. Their *n* values at 632.8 nm ($n_{632.8}$) were in the range of 1.686–1.621, which were much higher than common polymer such as polystyrene, polycarbonate, poly(methyl methacrylate), and polyacrylate with $n_{632.8}$ in the region of 1.49–1.58.[49]

The generation of fluorescent patterns by photolithography technique is of great significance in terms of the photonic and electronic applications.[50-52] As shown in Figure 2F–H, after irradiation by UV light in air for 20 min through a copper photomask, the fluorescence of the exposed regions (lines) was completely quenched due to the photo-oxidation of the chromophores, while the emissive squares were protected by copper and remained intact. Thus, two-dimensional fluorescent patterns with different emissive colors were generated with high resolution and sharp edges. By changing the shape and scale of the photomask, various patterns in different scales could be generated, such as QR code, which could be used for information storage (Figure 2I). Herein, these azonia-containing polyelectrolytes were expected to be promising materials for pattern fabrication, which would have profound implications in constructing electronic and photonic devices and various hybrid devices as excellent luminescent photoresist materials in a cost-efficient photolithography process. The photostability result showed that these polyelectrolytes were stable under the exposure of normal room light (Figure S13-14), and were also able to undergo photo-oxidative bleaching process with tunable refractive index under the exposure of strong UV light source (Figure S16, Table S3).

ROS Generation. The unique azonia moiety in these polymers encouraged us to explore their ROS generation ability and application in bacteria killing.[53-55] H2DCF-DA is a commercial ROS indicator, which is non-fluorescent but emits green fluorescence when oxidized by ROS.[56] H2DCF-DA was utilized to investigate the ROS generation ability of these azonia-containing polyelectrolytes, and P**1a/2e/3a**, P**1a/2d/3a**, and P**1a/2c/3a** were chosen for demonstration. As shown in Figure S10, in the mixture of polyelectrolytes and H2DCF-DA, the fluorescence intensity of H2DCF-DA at 525 nm increased gradually with the extension of irradiation time. A steeper slope of curves indicated much higher ROS generation rate, suggesting that three polyelectrolytes exhibited different ROS generation efficiency in the order of P**1a/2e/3a** > P**1a/2d/3a** > P**1a/2c/3a**.

Among all the ROS species, such as superoxide ($O_2^{\bullet-}$), hydrogen peroxide (H_2O_2), hydroxyl radical ($^{\bullet}OH$), and singlet oxygen ($^1O_2$), $^1O_2$ is regarded as a primary cytotoxic agent.[57] Herein, 9,10-anthracenediyl-bis-(methylene)-dimalonic acid (ABDA), a specific probe to detect $^1O_2$ was utilized to prove the generation of $^1O_2$ from azonia-containing polyelectrolytes.[58] In the presence of $^1O_2$, ABDA is transformed into endoperoxide, leading to a decrease of ABDA absorption at 378 nm. The absorbance spectra of ABDA solution in the presence of P**1a/2c/3a**, P**1a/2d/3a**, and P**1a/2e/3a** was recorded upon white light irradiation (Figure 3A–C). In the presence of these polyelectrolytes, noticeable reduction of ABDA absorption was observed, especially for P**1a/2e/3a**, which caused fastest drop of ABDA absorption (Figure 3D). For comparison, a commercial dye, Rose Bengal, which was widely used to generate $^1O_2$ with singlet oxygen quantum yield of 75%, was investigated under the same condition (Figure S11-12). The decomposition rates of ABDA in the presence of polyelectrolytes and Rose Bengal were calculated quantificationally (Figure 3D) and the results indicated that P**1a/2e/3a** was able to generate $^1O_2$ much more effectively than Rose Bengal. Such strong $^1O_2$ generation ability of P**1a/2e/3a** was probably due to the extended conjugation length between donor and acceptor, which minimized the ΔE_{ST} and enhanced the possibility of ISC process. Also, the strong D-A conjugated structure of P**1a/2e/3a** rigidified its polymer backbone, which could minimize its nonradiative decay and thus promote the ISC process. The photostability study showed that P**1a/2e/3a** indicated better photostability than organic dyes RB and 5,10,15,20-tetrakis(4-sulfonatophenyl)-porphyrin (TPPS), two traditional photosensitizers generally employed for PDT (Figure S15).

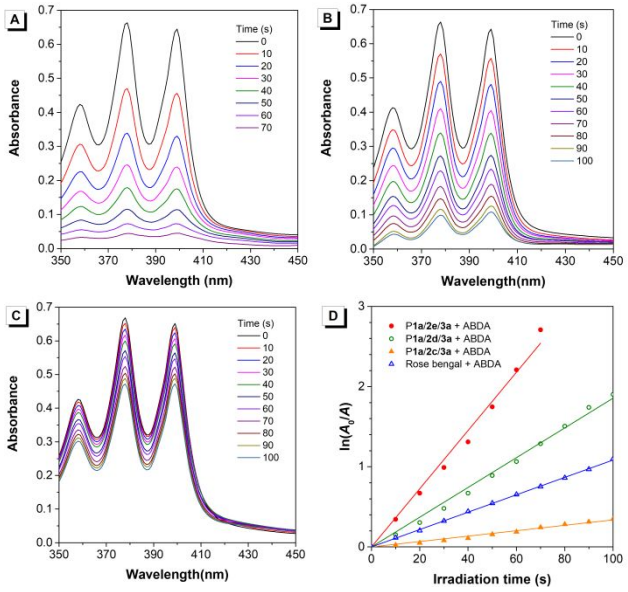

Figure 3. (A-C) UV-vis absorption spectra of ABDA in the presence of (A) P**1a/2e/3a**, (B) P**1a/2d/3a** and (C) P**1a/2c/3a**. (D) The decomposition rates of ABDA by P**1/2/3** and rose Bengal where A_0 and A are the absorbance of ABDA in the presence of PSs at 378 nm before and after irradiation, respectively.

Superbug Killing. The strong $^1O_2$ generation ability of these polyelectrolytes motivated us to further explore its performance as photosensitizer in bacteria inhibition. P**1a/2e/3a** with most significant ROS generation was chosen for further biological evaluation. The hydrodynamic diameter of P**1a/2e/3a** micelles was determined to be ~106 nm by dynamic laser scattering (DLS) analysis, and the transmission electron microscopy (TEM) analysis confirmed the spherical morphology and size (Figure 4A). Then, *in vitro* antimicrobial activities of P**1a/2e/3a** were firstly evaluated towards representative Gram-positive *S. aureus* and Gram-negative *E. coli*, respectively (Figure S18). The polymer showed weak inhibition to *E. coli* even under light irradiation, but strong inhibition to *S. aureus* under white light irradiation with minimal inhibition concentration (MIC) of 15 ug/mL. The different antimicrobial ability was probably due to the membrane difference between Gram-negative bacteria and Gram-

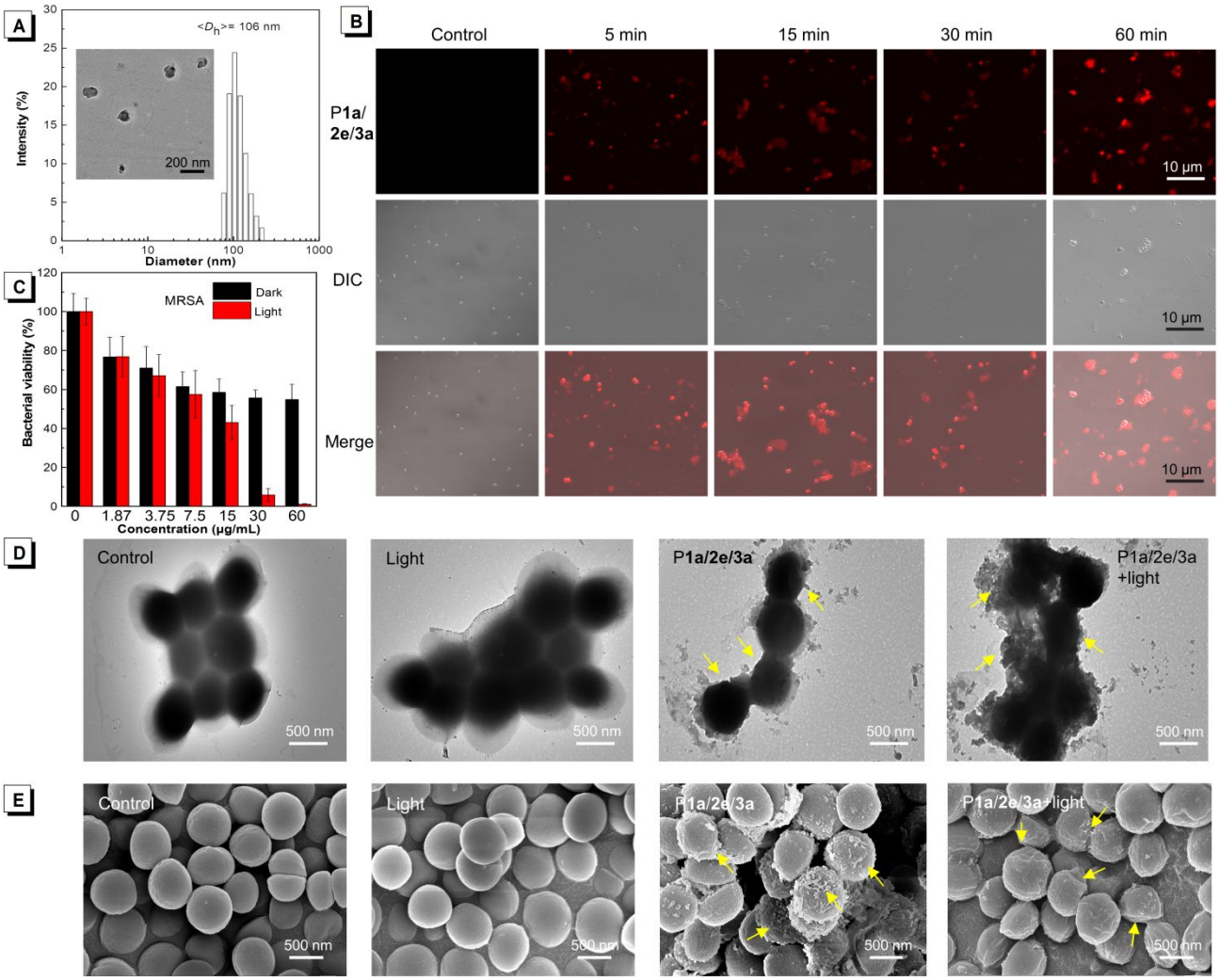

Figure 4. (A) Hydrodynamic diameter distribution and TEM image of P**1a**/**2e**/**3a** aqueous suspension. (B) Fluorescent images, DIC images and their merge images of MRSA upon treatment with P**1a**/**2e**/**3a**. (C) Quantitative antibacterial tests of P**1a**/**2e**/**3a** against MRSA in the presence or absence of light irradiation. (D) Morphology change of MRSA upon diverse treatments observed by TEM. (E) Morphology change of MRSA upon diverse treatments observed by SEM.

positive bacteria, it was difficult for polymer micelles to access membrane of Gram-negative bacteria due to its extra protective membrane components.[39] Notably, undetectable ROS generation of monomers **1a**, **2e**, and **3a** was also proved by the chemical trapping measurements with ABDA as indicator (Figure S17).

MRSA is one of the most notorious drug-resistant Gram-positive bacteria in the hospital environment and community settings, leading to a variety of clinical syndromes such as endocarditis, pneumonia, and central nervous system infections.[59-61] As the polyelectrolyte P**1a**/**2e**/**3a** showed good inhibition to Gram-positive *S. aureus*, thus the inhibition potency against MRSA were evaluated to further explore its antimicrobial ability against drug-resistant bacteria. As shown in Figure 4B, the high charge density in the polymer main chain enabled P**1a**/**2e**/**3a** to possess high affinity to negatively charged bacteria membrane, thus could stain MRSA quickly, as short as 5 min. Furthermore, persistent fluorescence was found for bacteria even upon incubation for 60 min, which was favorable for extended light irradiation.

After that, the quantitative MRSA inhibition of P**1a**/**2e**/**3a** was performed in the presence of light irradiation or not (Figure 4C). In dark state, P**1a**/**2e**/**3a** exhibited moderate inhibition against MRSA, as the positive charges on the polyelectrolyte main chain enabled the micelles to adhere and fuse with the bacteria membrane, thus physically damaged bacteria membrane to some extent.[62] Upon white light irradiation, P**1a**/**2e**/**3a** could generate $^1O_2$ efficiently apart from the physical damage effect, leading to much stronger inhibition against MRSA with an MIC value of ~30 ug/mL. In addition, the raw monomers **1a**, **2e**, and **3a** of P**1a**/**2e**/**3a** all exhibited minimal bacteria inhibition even in the presence of light irradiation, which further highlighted advantageous P**1a**/**2e**/**3a** with remarkable PDT potency (Figure S19)

Furthermore, the morphology change of MRSA upon diverse treatments was observed by TEM and SEM analysis (Figure 4D-E). After incubation at 37 °C for 30 min, both the control sample and single light-treating sample exhibited smooth membrane surface and intact membrane structure, while the cell surface of MRSA became rough and out of

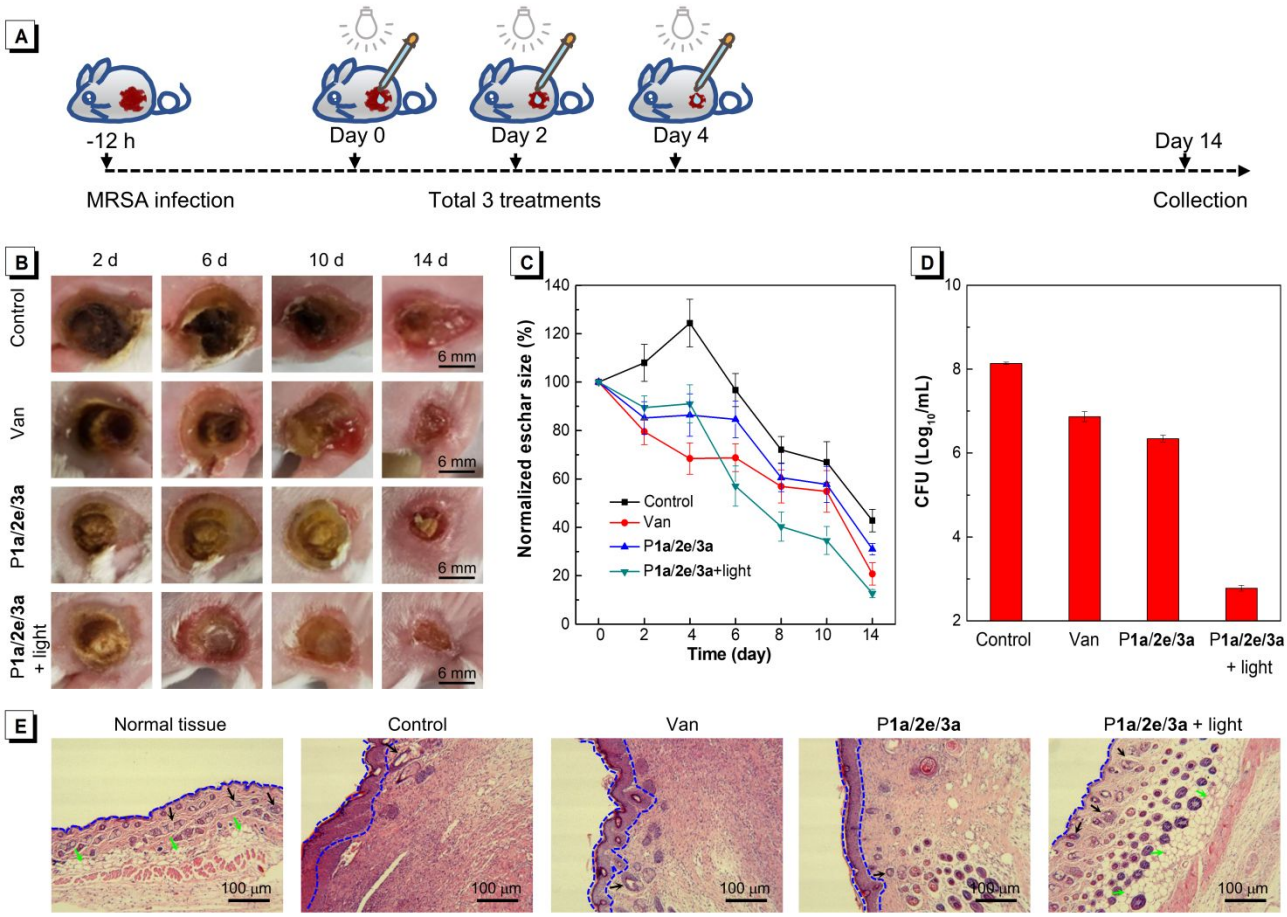

Figure 5. (A) Schematic illustration for the construction of MRSA-infected mouse burn model and the therapeutic profile. (B) Typical photographs of MRSA-infected burn sites upon different treatments under dark or light irradiation during the therapeutic processes. (C) Relative eschar size analysis after diverse treatments at the 14th day. (D) The number of MRSA in the infected tissues was quantified at the 14th day. (E) Histologic analysis of the MRSA-infected burn injury tissue by hematoxylin and eosin staining for different treatment groups. As a comparison, commercial vancomycin was evaluated in parallel. Blue dotted lines indicate the epithelium border, green arrows show the adipose cells and black arrows present the hair follicles.

shape under the treatment of P**1a/2e/3a** in dark state, many micelles were found to be around the bacteria, demonstrating efficient binding, adhesion and further fusion with MRSA membrane. Finally, as the yellow arrows indicated, much more significant membrane shrinking and deformation were observed upon micelles binding and extra light irradiation.

To investigate the biocompatibility of the polyelectrolytes, MTT assays were performed for P**1a/2e/3a** upon incubation with primary skin fibroblast cells for 24 h. P**1a/2e/3a** showed undetectable toxicity toward the cells even up to 175 μg/mL under light irradiation (Figure S20), exhibiting good biocompatibility and antibacterial selectivity, which was favorable for *in vivo* applications.

In vivo bacteria inhibition experiment was conducted on a MRSA-infected mouse burn model.[63] Different treatments were applied to the MRSA-infected burn sites, and the recovery process was evaluated in 14 days (Figure 5A). Effectively accelerated would healing process was observed when treated with vancomycin or P**1a/2e/3a** with light irradiation, as compared to the control group (Figure 5B-C). After the whole treating process in 14 days, the mice were sacrificed, and their wound tissues were harvested for further evaluation. Although vancomycin could also enhance the wound healing process, the quantitative experiments showed that the inhibition effect of P**1a/2e/3a** under white light irradiation was much better than vancomycin, the golden standard for Gram-positive bacteria treatment (Figure 5D, Figure S21). Histologic analysis was conducted to further evaluate the treatment effect (Figure 5E). Normal mouse skin was highly heterogeneous tissue, containing epidermis, dermis with hair follicle, and subcutaneous layer. At the 14th day, the control group only showed partially re-epithelialized and thickened epidermis, while tissue of the P**1a/2e/3a** under light irradiation-treated group showed obvious re-epithelialized, exhibiting intact skin microstructure comparable with normal tissue. Thus, *in vivo* MRSA-infected mouse burn model demonstrated that the photodynamic effect of P**1a/2e/3a** could inhibit MRSA infection in the burn injury mouse model and effectively accelerate the healing process.

CONCLUSION

In summary, we have developed an efficient one-pot polymerization route to in-situ generate functional azonia-

containing polyelectrolytes using readily accessible nonionic reactants and commercially available cheap ionic species. Compared with traditional synthetic strategies of polyelectrolytes, this new strategy did not require post-modification step or expensive ionic monomers. The polymerization proceeded efficiently in air with high tolerance to the monomer feed ratio, generating polyelectrolytes in excellent yields (up to 99%) with high molecular weights (up to 28 700) in high atom economy. With electron-deficient azonia fused rings in the polymer main-chain, the emission color of resulting polyelectrolytes could be easily tuned by changing the electron donor. With high luminescence in solid state, good processing ability, and high refractive indices, these polymers were excellent materials for fluorescent photopatterns and promising for optical applications. Notably, the azonia-containing polyelectrolytes had strong ROS generation ability and could impressively kill the drug resistant superbug. P**1a/2e/3a** was demonstrated to effectively kill MRSA both *in vitro* and in the MRSA-infected mouse burn model. The efficient one-pot synthetic methodology to azonia-containing polyelectrolytes provided a new strategy for the synthesis of polyelectrolytes, greatly enriching the family of polyelectrolytes. Current charge-generating polymerization provided these prominent functional positively charged polyelectrolytes, which were promising candidates for various biomedical applications, such as tissue engineering, surface modification, and self-healing materials.

ASSOCIATED CONTENT

Supporting Information.

This material is available free of charge via the Internet at http://pubs.acs.org.

Details of the materials, methods, synthetic procedures, and characterization data (IR, NMR, TGA, DSC, etc.); photophysical properties, photo stability study, and light refraction data of the polymers; ROS-generation detection, quantitative antibacterial tests data, and MTT assays (PDF)

AUTHOR INFORMATION

Corresponding Author

* xlhu@scnu.edu.cn, huxlong@mail.ustc.edu.cn
* chjacky@ust.hk
* tangbenz@ust.hk

ORCID

Xiaolin Liu: 0000-0002-6909-117X
Xianglong Hu: 0000-0001-9202-1543
Ben Zhong Tang: 0000-0002-0293-964X

Author Contributions

#X.L. and M.L. contributed equally to this work.

Notes

The authors declare no competing financial interest.

ACKNOWLEDGMENT

This work was financially supported by the National Science Foundation of China (21788102, and 21674040), the Research Grants Council of Hong Kong (16308116, C6009-17G and A-HKUST605/16), the Innovation and Technology Commission (ITC-CNERC14SC01 and ITS/254/17), the National Key Research and Development program of China (2018YFE0190200), the Science and Technology Plan of Shenzhen (JCYJ20170818113530705 and JCYJ20180306180231853), the Natural Science Foundation for Distinguished Young Scholars of Guangdong Province (2016A030306013), and the Pearl River Young Talents Program of Science and Technology in Guangzhou (201906010047).

REFERENCES

(1) Fuoss, R. M., Polyelectrolytes. *Science* **1948,** *108* (2812), 545-550.

(2) Regelson, W.; Kuhar, S.; Tunis, M.; Fields, J.; Johnson, J.; Gluesenkamp, E., Synthetic Polyelectrolytes as Tumour Inhibitors. *Nature* **1960,** *186* (4727), 778-780.

(3) Rubinstein, M.; Papoian, G. A., Polyelectrolytes in Biology and Soft Matter. *Soft Matter* **2012,** *8* (36), 9265-9267.

(4) Li, X.; Bai, H.; Yang, Y.; Yoon, J.; Wang, S.; Zhang, X., Supramolecular Antibacterial Materials for Combatting Antibiotic Resistance. *Adv. Mater.* **2019,** *31* (5), 1805092.

(5) Meka, V. S.; Sing, M. K.; Pichika, M. R.; Nali, S. R.; Kolapalli, V. R.; Kesharwani, P., A Comprehensive Review on Polyelectrolyte Complexes. *Drug Discovery Today* **2017,** *22* (11), 1697-1706.

(6) Laschewsky, A., Recent Trends in the Synthesis of Polyelectrolytes. *Curr. Opin. Colloid Interface Sci.* **2012,** *17* (2), 56-63.

(7) Mortimer, D. A., Synthetic Polyelectrolytes—a Review. *Polym. Int.* **1991,** *25* (1), 29-41.

(8) Laschewsky, A., Structures and Synthesis of Zwitterionic Polymers. *Polymers* **2014,** *6* (5), 1544-1601.

(9) Eftekhari, A.; Saito, T., Synthesis and Properties of Polymerized Ionic Liquids. *Eur. Polym. J.* **2017,** *90*, 245-272.

(10) Sen, A. K.; Roy, S.; Juvekar, V. A., On the Importance of Purification of Sodium Polystyrene Sulfonate. *ISRN Anal. Chem.* **2012,** *2012*.

(11) Tran, Y.; Auroy, P., Synthesis of Poly (Styrene Sulfonate) Brushes. *J. Am. Chem. Soc.* **2001,** *123* (16), 3644-3654.

(12) Hua, F.; Kita, R.; Wegner, G.; Meyer, W., Interactions between Brushlike Polyacrylic Acid Side Chains on a Polyacrylate Backbone in Dioxane–Water. *ChemPhysChem* **2005,** *6* (2), 336-343.

(13) Mori, H.; Müller, A. H., New Polymeric Architectures with (Meth) Acrylic Acid Segments. *Prog. Polym. Sci.* **2003,** *28* (10), 1403-1439.

(14) Zhu, C.; Yang, Q.; Liu, L.; Wang, S., A Potent Fluorescent Probe for the Detection of Cell Apoptosis. *Chem. Commun.* **2011,** *47* (19), 5524-5526.

(15) Moon, J. H.; McDaniel, W.; MacLean, P.; Hancock, L. F., Live-Cell-Permeable Poly (P-Phenylene Ethynylene). *Angew. Chem.* **2007,** *119* (43), 8371-8373.

(16) Xiang, T.; Wang, L.-R.; Ma, L.; Han, Z.-Y.; Wang, R.; Cheng, C.; Xia, Y.; Qin, H.; Zhao, C.-S., From Commodity Polymers to Functional Polymers. *Sci. Rep.* **2014,** *4*, 4604.

(17) Lemstra, P. J.; Kirschbaum, R., Speciality Products Based on Commodity Polymers. *Polymer* **1985,** *26* (9), 1372-1384.

(18) Fan, J.; Borguet, Y. P.; Su, L.; Nguyen, T. P.; Wang, H.; He, X.; Zou, J.; Wooley, K. L., Two-Dimensional Controlled Syntheses of Polypeptide Molecular Brushes Via N-Carboxyanhydride Ring-Opening Polymerization and Ring-Opening Metathesis Polymerization. *ACS Macro Lett.* **2017,** *6* (9), 1031-1035.

(19) Nicholson, J. W., Polyelectrolyte Materials – Reflections on a Highly Charged Topic. *Chem. Soc. Rev.* **1994,** *23* (1), 53-58.

(20) Jiang, Y.; Freyer, J. L.; Cotanda, P.; Brucks, S. D.; Killops, K. L.; Bandar, J. S.; Torsitano, C.; Balsara, N. P.; Lambert, T. H.; Campos, L. M., The Evolution of Cyclopropenium Ions into Functional Polyelectrolytes. *Nat. Commun.* **2015,** *6*, 5950.

(21) Zhu, T.; Sha, Y.; Yan, J.; Pageni, P.; Rahman, M. A.; Yan, Y.; Tang, C., Metallo-Polyelectrolytes as a Class of Ionic Macromolecules for Functional Materials. *Nat. Commun.* **2018,** *9* (1), 4329.

(22) Zhu, T.; Xu, S.; Rahman, A.; Dogdibegovic, E.; Yang, P.; Pageni, P.; Kabir, M. P.; Zhou, X.-d.; Tang, C., Cationic Metallo-Polyelectrolytes for Robust Alkaline Anion-Exchange Membranes. *Angew. Chem., Int. Ed.* **2018,** *57* (9), 2388-2392.

(23) Li, Y.; Du, W.; Sun, G.; Wooley, K. L., Ph-Responsive Shell Cross-Linked Nanoparticles with Hydrolytically Labile Cross-Links.

Macromolecules **2008,** *41* (18), 6605-6607.
(24) Jiang, H.; Taranekar, P.; Reynolds, J. R.; Schanze, K. S., Conjugated Polyelectrolytes: Synthesis, Photophysics, and Applications. *Angew. Chem., Int. Ed.* **2009,** *48* (24), 4300-4316.
(25) Zhu, C.; Liu, L.; Yang, Q.; Lv, F.; Wang, S., Water-Soluble Conjugated Polymers for Imaging, Diagnosis, and Therapy. *Chem. Rev.* **2012,** *112* (8), 4687-4735.
(26) Elsabahy, M.; Heo, G. S.; Lim, S.-M.; Sun, G.; Wooley, K. L., Polymeric Nanostructures for Imaging and Therapy. *Chem. Rev.* **2015,** *115* (19), 10967-11011.
(27) Pu, K.-Y.; Liu, B., Fluorescent Conjugated Polyelectrolytes for Bioimaging. *Adv. Funct. Mater.* **2011,** *21* (18), 3408-3423.
(28) Yuan, H.; Liu, Z.; Liu, L.; Lv, F.; Wang, Y.; Wang, S., Cationic Conjugated Polymers for Discrimination of Microbial Pathogens. *Adv. Mater.* **2014,** *26* (25), 4333-4338.
(29) Hu, F.; Xu, S.; Liu, B., Photosensitizers with Aggregation-Induced Emission: Materials and Biomedical Applications. *Adv. Mater.* **2018,** *30* (45), 1801350.
(30) Zhu, C.; Kwok, R. T. K.; Lam, J. W. Y.; Tang, B. Z., Aggregation-Induced Emission: A Trailblazing Journey to the Field of Biomedicine. *ACS Appl. Bio Mater.* **2018,** *1* (6), 1768-1786.
(31) Jiang, M.; Kwok, R. T.; Li, X.; Gui, C.; Lam, J. W.; Qu, J.; Tang, B. Z., A Simple Mitochondrial Targeting Aiegen for Image-Guided Two-Photon Excited Photodynamic Therapy. *J. Mater. Chem. B* **2018,** *6* (17), 2557-2565.
(32) Jiang, M.; Gu, X.; Kwok, R. T.; Li, Y.; Sung, H. H.; Zheng, X.; Zhang, Y.; Lam, J. W.; Williams, I. D.; Huang, X., Multifunctional Aiegens: Ready Synthesis, Tunable Emission, Mechanochromism, Mitochondrial, and Bacterial Imaging. *Adv. Funct. Mater.* **2018,** *28* (1), 1704589.
(33) Wang, D.; Lee, M. M.; Shan, G.; Kwok, R. T.; Lam, J. W.; Su, H.; Cai, Y.; Tang, B. Z., Highly Efficient Photosensitizers with Far-Red/near-Infrared Aggregation-Induced Emission for in Vitro and in Vivo Cancer Theranostics. *Adv. Mater.* **2018,** *30* (39), 1802105.
(34) Zhang, T.; Li, Y.; Zheng, Z.; Ye, R.; Zhang, Y.; Kwok, R. T. K.; Lam, J. W. Y.; Tang, B. Z., In Situ Monitoring Apoptosis Process by a Self-Reporting Photosensitizer. *J. Am. Chem. Soc.* **2019,** *141* (14), 5612-5616.
(35) Yin, J.; Tan, M.; Wu, D.; Jiang, R.; Li, C.; You, J., Synthesis of Phenalenyl-Fused Pyrylium Cations: Divergent C–H Activation/Annulation Reaction Sequence of Naphthalene Aldehydes with Alkynes. *Angew. Chem., Int. Ed.* **2017,** *56* (42), 13094-13098.
(36) Bica, K.; Rijksen, C.; Nieuwenhuyzen, M.; Rogers, R. D., In Search of Pure Liquid Salt Forms of Aspirin: Ionic Liquid Approaches with Acetylsalicylic Acid and Salicylic Acid. *Phys. Chem. Chem. Phys.* **2010,** *12* (8), 2011-2017.
(37) Cao, B.; Xiao, F.; Xing, D.; Hu, X. L., Polyprodrug Antimicrobials: Remarkable Membrane Damage and Concurrent Drug Release to Combat Antibiotic Resistance of Methicillin-Resistant Staphylococcus Aureus. *Small* **2018,** *14* (41), 1802008.
(38) Wang, B.; Yuan, H.; Liu, Z.; Nie, C.; Liu, L.; Lv, F.; Wang, Y.; Wang, S., Cationic Oligo (P-Phenylene Vinylene) Materials for Combating Drug Resistance of Cancer Cells by Light Manipulation. *Adv. Mater.* **2014,** *26* (34), 5986-5990.
(39) Xiao, F.; Cao, B.; Wang, C.; Guo, X.; Li, M.; Xing, D.; Hu, X. L., Pathogen-Specific Polymeric Antimicrobials with Significant Membrane Disruption and Enhanced Photodynamic Damage to Inhibit Highly Opportunistic Bacteria. *ACS Nano* **2019,** *13* (2), 1511-1525.
(40) Wang, B.; Wang, M.; Mikhailovsky, A.; Wang, S.; Bazan, G. C., A Membrane-Intercalating Conjugated Oligoelectrolyte with High-Efficiency Photodynamic Antimicrobial Activity. *Angew. Chem., Int. Ed.* **2017,** *56* (18), 5031-5034.
(41) Sucunza, D.; Cuadro, A. M.; Alvarez-Builla, J.; Vaquero, J. J., Recent Advances in the Synthesis of Azonia Aromatic Heterocycles. *J. Org. Chem.* **2016,** *81* (21), 10126-10135.
(42) Fu, G. C.; Grubbs, R. H., The Application of Catalytic Ring-Closing Olefin Metathesis to the Synthesis of Unsaturated Oxygen Heterocycles. *J. Am. Chem. Soc.* **1992,** *114* (13), 5426-5427.
(43) Abengozar, A.; Abarca, B.; Cuadro, A. M.; Sucunza, D.; Alvarez-Builla, J.; Vaquero, J. J., Azonia Aromatic Cations by Ring-Closing Metathesis: Synthesis of Azaquinolizinium Cations. *Eur. J. Org. Chem.* **2015,** *2015* (19), 4214-4223.
(44) Prakash, S.; Muralirajan, K.; Cheng, C. H., Cobalt-Catalyzed Oxidative Annulation of Nitrogen-Containing Arenes with Alkynes: An Atom-Economical Route to Heterocyclic Quaternary Ammonium Salts. *Angew. Chem., Int. Ed.* **2016,** *55* (5), 1844-1848.
(45) Ge, Q.; Hu, Y.; Li, B.; Wang, B., Synthesis of Conjugated Polycyclic Quinoliniums by Rhodium (Iii)-Catalyzed Multiple C–H Activation and Annulation of Arylpyridiniums with Alkynes. *Org. Lett.* **2016,** *18* (10), 2483-2486.
(46) Toriumi, N.; Asano, N.; Miyamoto, K.; Muranaka, A.; Uchiyama, M., N-Alkynylpyridinium Salts: Highly Electrophilic Alkyne–Pyridine Conjugates as Precursors of Cationic Nitrogen-Embedded Polycyclic Aromatic Hydrocarbons. *J. Am. Chem. Soc.* **2018,** *140* (11), 3858-3862.
(47) Han, Y. R.; Shim, S.-H.; Kim, D.-S.; Jun, C.-H., Synthesis of Benzoquinolizinium Salts by Rh (Iii)-Catalyzed Cascade Double N-Annulation Reactions of Allylamines, Diarylacetylenes, and Hbf4. *Org. Lett.* **2017,** *19* (11), 2941-2944.
(48) Higashihara, T.; Ueda, M., Recent Progress in High Refractive Index Polymers. *Macromolecules* **2015,** *48* (7), 1915-1929.
(49) Hiorns, R., Polymer Handbook, 4th Edn, Edited by J Brandup, Eh Immergut and Ea Grulke, Associate Editors a Abe and Dr Bloch, John Wiley and Sons, New York, 1999, Pp 2250, Price £210 Isbn 0-471-16628-6. *Polym. Int.* **2000,** *49* (7), 807-807.
(50) Wang, Y.; Fedin, I.; Zhang, H.; Talapin, D. V., Direct Optical Lithography of Functional Inorganic Nanomaterials. *Science* **2017,** *357* (6349), 385-388.
(51) Perry, J. W., Two Beams Squeeze Feature Sizes in Optical Lithography. *Science* **2009,** *324* (5929), 892-893.
(52) Wang, Q. H.; Jin, Z.; Kim, K. K.; Hilmer, A. J.; Paulus, G. L. C.; Shih, C.-J.; Ham, M.-H.; Sanchez-Yamagishi, J. D.; Watanabe, K.; Taniguchi, T.; Kong, J.; Jarillo-Herrero, P.; Strano, M. S., Understanding and Controlling the Substrate Effect on Graphene Electron-Transfer Chemistry Via Reactivity Imprint Lithography. *Nat. Chem.* **2012,** *4*, 724.
(53) Yu, C. Y.; Xu, H.; Ji, S.; Kwok, R. T.; Lam, J. W.; Li, X.; Krishnan, S.; Ding, D.; Tang, B. Z., Mitochondrion-Anchoring Photosensitizer with Aggregation-Induced Emission Characteristics Synergistically Boosts the Radiosensitivity of Cancer Cells to Ionizing Radiation. *Adv. Mater.* **2017,** *29* (15), 1606167.
(54) You, X.; Ma, H.; Wang, Y.; Zhang, G.; Peng, Q.; Liu, L.; Wang, S.; Zhang, D., Pyridinium-Substituted Tetraphenylethyleneentailing Alkyne Moiety: Enhancement of Photosensitizing Efficiency and Antimicrobial Activity. *Chem. - Asian J.* **2017,** *12* (9), 1013-1019.
(55) Zhang, C.-J.; Hu, Q.; Feng, G.; Zhang, R.; Yuan, Y.; Lu, X.; Liu, B., Image-Guided Combination Chemotherapy and Photodynamic Therapy Using a Mitochondria-Targeted Molecular Probe with Aggregation-Induced Emission Characteristics. *Chem. Sci.* **2015,** *6* (8), 4580-4586.
(56) Zheng, Z.; Zhang, T.; Liu, H.; Chen, Y.; Kwok, R. T. K.; Ma, C.; Zhang, P.; Sung, H. H. Y.; Williams, I. D.; Lam, J. W. Y.; Wong, K. S.; Tang, B. Z., Bright near-Infrared Aggregation-Induced Emission Luminogens with Strong Two-Photon Absorption, Excellent Organelle Specificity, and Efficient Photodynamic Therapy Potential. *ACS Nano* **2018,** *12* (8), 8145-8159.
(57) Kearns, D. R., Physical and Chemical Properties of Singlet Molecular Oxygen. *Chem. Rev.* **1971,** *71* (4), 395-427.
(58) Zhu, C.; Yang, Q.; Liu, L.; Lv, F.; Li, S.; Yang, G.; Wang, S., Multifunctional Cationic Poly(P-Phenylene Vinylene) Polyelectrolytes for Selective Recognition, Imaging, and Killing of Bacteria over Mammalian Cells. *Adv. Mater.* **2011,** *23* (41), 4805-4810.
(59) Courtney, C. M.; Goodman, S. M.; McDaniel, J. A.; Madinger, N. E.; Chatterjee, A.; Nagpal, P., Photoexcited Quantum Dots for Killing Multidrug-Resistant Bacteria. *Nat. Mater.* **2016,** *15*, 529.
(60) Chin, W.; Zhong, G.; Pu, Q.; Yang, C.; Lou, W.; De Sessions, P. F.; Periaswamy, B.; Lee, A.; Liang, Z. C.; Ding, X.; Gao, S.; Chu, C. W.; Bianco, S.; Bao, C.; Tong, Y. W.; Fan, W.; Wu, M.; Hedrick, J. L.; Yang, Y. Y., A Macromolecular Approach to Eradicate Multidrug Resistant Bacterial Infections While Mitigating Drug Resistance Onset. *Nat. Commun.* **2018,** *9* (1), 917.
(61) Wu, C.; Shang, Z.; Lemetre, C.; Ternei, M. A.; Brady, S. F., Cadasides, Calcium-Dependent Acidic Lipopeptides from the Soil Metagenome That Are Active against Multidrug-Resistant Bacteria. *J. Am. Chem. Soc.* **2019,** *141* (9), 3910-3919.
(62) Engler, A. C.; Wiradharma, N.; Ong, Z. Y.; Coady, D. J.; Hedrick, J. L.; Yang, Y.-Y., Emerging Trends in Macromolecular Antimicrobials to Fight Multi-Drug-Resistant Infections. *Nano Today* **2012,** *7* (3), 201-222.
(63) Li, Y.; Liu, G.; Wang, X.; Hu, J.; Liu, S., Enzyme-Responsive Polymeric Vesicles for Bacterial-Strain-Selective Delivery of Antimicrobial Agents. *Angew. Chem., Int. Ed.* **2016,** *55* (5), 1760-1764.

For Table of Contents Only